Plasmonic Stripes in Aqueous Environment Co-Integrated With Si₃N₄ Photonics

George Dabos
Dimitra Ketzaki
Athanasios Manolis
Laurent Markey
Jean Claude Weeber
Alain Dereux
Anna Lena Giesecke
Caroline Porschatis
Bartos Chmielak
Dimitris Tsiokos
Nikos Pleros
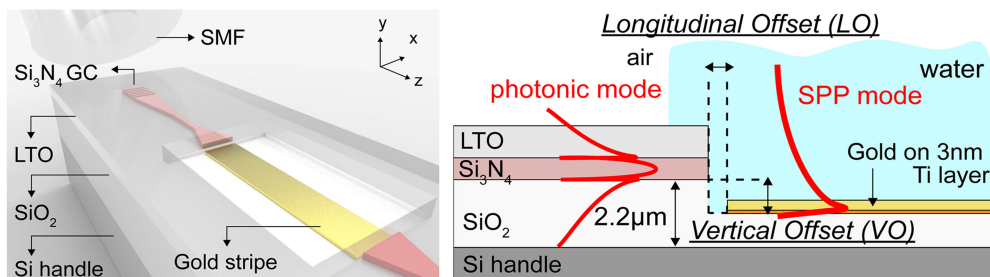
Plasmonic Stripes in Aqueous Environment Co-Integrated With Si$_3$N$_4$ Photonics

George Dabos [ORCID],[1] **Dimitra Ketzaki,**[1] **Athanasios Manolis,**[1]
Laurent Markey,[2] **Jean Claude Weeber,**[2] **Alain Dereux,**[2]
Anna Lena Giesecke,[3] **Caroline Porschatis,**[3] **Bartos Chmielak,**[3]
Dimitris Tsiokos,[1] **and Nikos Pleros [ORCID]** [1]

[1]Department of Informatics, Center for Interdisciplinary Research and Innovation, Aristotle University of Thessaloniki, Thessaloniki 57001, Greece
[2]Laboratoire Interdisciplinaire Carnot de Bourgogne, UMR 6303 CNRS-Université de Bourgogne, Dijon 21078, France
[3]AMO GmbH, Advanced Microelectronic Center Aachen, Aachen 52074, Germany

Abstract: We demonstrate the design, fabrication, and the experimental characterization of gold-based plasmonic stripes butt-coupled with low-pressure-chemical-vapor-deposition (LPCVD)-based Si$_3$N$_4$ waveguides for the excitation of surface-plasmon-polariton (SPP) modes in aqueous environment. Plasmonic gold stripes, in aqueous environment, with cross-sectional dimensions of 100 nm $\times$ 7 μm were interfaced with 360 nm $\times$ 800 nm Si$_3$N$_4$ waveguides cladded with low-temperature-oxide, exploiting linear photonic tapers with appropriate vertical (VO) and longitudinal (LO) offsets between the plasmonic and photonic waveguide facets. An interface insertion loss of 2.3 $\pm$ 0.3 dB and a plasmonic propagation length (L_{spp}) of 75 μm have been experimentally measured at 1.55 μm for a VO of 400 nm and an LO of 500 nm, with simulation results suggesting high tolerance to VO and LO misalignment errors. The proposed integration approach enables seamless co-integration of plasmonic stripes, in aqueous environment, with a low-loss and low-cost LPCVD-based Si$_3$N$_4$ waveguide platform, revealing its strong potential for future employment in biochemical sensing applications.

Index Terms: Photonic integrated circuits, plasmonics, surface plasmons, butt-coupled interface, plasmonic waveguide.

1. Introduction

Plasmonics were introduced as a highly promising candidate that may revolutionize photonic-integrated-circuits (PICs), unleashing unprecedented performance breakthroughs in diverse application areas [1]. Harnessing the unique capability of plasmonic waveguides to guide light at metal surfaces can offer a number of unmatched advantages: i) sub-wavelength confinement of SPP modes, (ii) interface with electronics due to the metallic waveguide nature, (iii) increased light–matter interaction as a result of the SPP confinement at the metal surface, and (iv) the capability to employ different materials as cladding and tailor the waveguide characteristics depending on the

desired application. In this context, SPP waveguides can be configured [2]–[7] to address different applications spanning from optical interconnects [8], [9], active nanophotonic components [10]–[15], to on-chip biochemical sensing [16]–[19].

However, the inherent high propagation losses of SPP waveguide configurations impede their broad utilization in more complicated PICs. To lower this barrier, plasmonic structures may be selectively co-integrated with low-loss photonic waveguides therefore minimizing chip losses coming from plasmonic sections while reaping the benefits of guiding light over metal surfaces. Co-integrating the two waveguide platforms allows the use of plasmonics on chip, only where their functional benefits are unmatched, complemented with low-loss photonic structures for the additional necessary circuitry. Merging plasmonics with photonics in a common integration platform has been so far demonstrated in a range of waveguide configurations and functional devices, exploiting mostly silicon [20]–[25] but also silicon nitride [26]–[28] as the photonic waveguide platform. However, only a limited number of plasmo-photonic interface structures has been proposed when plasmonic propagation in aqueous environment is required [29], [30], as is typically the case when biochemical sensing applications are targeted. A hybrid double slot plasmonic waveguide co-integrated with silicon has been presented in [29] while the use of the lower loss SiN waveguide platform as the photonic host has been employed only in a vertically coupled scheme with an ultra-thin SPP metallic stripe being cladded with water [30], exploiting the directional coupling mechanism to excite Short-Range SPP modes at the ultra-thin plasmonic stripe. The vertical coupling approach relies on a SiO_2 buffer layer located between the SiN and the SPP waveguides, however, a 300 nm deviation of the optimal SiO_2 buffer thickness has been shown theoretically by the same group to increase coupling losses by more than 3 dB [27].

In this paper, we present for the first time to the best of our knowledge, the co-integration of gold-based plasmonic stripes and LPCVD-based Si_3N_4 waveguides using a butt-coupled interface and supporting propagating SPP modes in aqueous environment. The proposed interface was designed and fabricated considering a 360 nm $\times$ 800 nm Si_3N_4 waveguide platform cladded with LTO and tapered to water-cladded gold stripes with cross-sectional dimensions of 100 nm $\times$ 7 μm and length between 20 to 250 μm. A cavity was defined using i-line stepper lithography between the two Si_3N_4 waveguides to allow the gold stripe deposition. Experimental measurements revealed good agreement with theoretically predicted values, demonstrating photonic-to-plasmonic interface coupling losses of 2.3 dB for a vertical offset (VO) of 400 nm between the two waveguide facets, and plasmonic propagation losses of 0.058 dB/μm at 1.55 μm in aqueous environment, which corresponds to a plasmonic propagation length L_{spp} of 75 μm. Numerical modelling results revealed an increased tolerance to both the VO and the longitudinal offset (LO) values, indicating an excessive loss of only 0.3 dB for a VO range between 300–700 nm and an excessive loss of only 0.5 dB when the LO ranges between 300–700 μm. To this end, the proposed platform can facilitate fabrication-tolerant co-integration of low-loss LPCVD-based silicon nitride photonics with propagating SPP modes in aqueous environment, potentially enabling its future exploitation in biochemical sensing applications.

The rest of the paper is organized as follows. In Section 2, we present the design and simulations performed utilizing a three-dimensional finite-difference-time-domain method (3D FDTD). Section 3 describes the fabrication process and the experimental results obtained by means of broadband optical characterization using a fiber-to-fiber configuration based on grating-couplers (GCs), with Section 4 providing concluding remarks and perspectives.

2. Design and Simulation

The proposed interface has been designed and numerically simulated employing a 3D-FDTD method from a commercial available package [31]. Fig. 1(a) depicts a conceptual schematic of the co-integrated plasmonic and Si_3N_4 waveguide platform, illustrating also the fiber-to-chip coupling that relied on an out-of-plane coupling scheme based on Si_3N_4 GCs [32], [33]. A side view of the butt-coupled interface is shown in Fig. 1(b), revealing that water has been used as the surrounding medium on top of the gold stripe. A vertical and a longitudinal offset (VO and LO, respectively) have been introduced at the photonic-to-plasmonic interface. The main purpose of the vertical
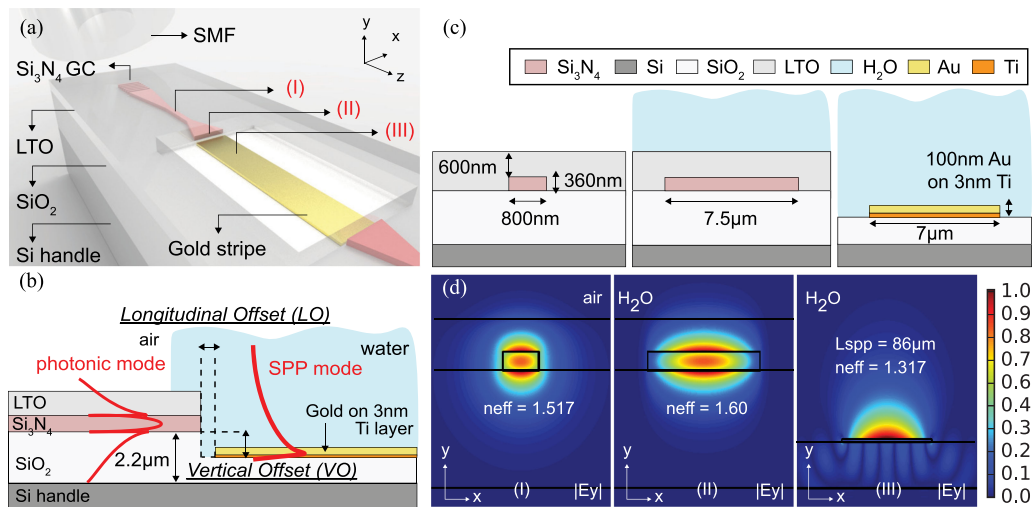
Fig. 1. (a) Conceptual schematic of the butt-coupled interface. The gold stripe is recessed within a cavity formed by etching in one step LTO, Si_3N_4 and SiO_2. The Ti layer underneath the gold and the water on top of the interface are not shown for clarity. Dimensions are not to scale. (b) Side-view of the proposed interface. (c) Cross-sectional dimensions for the photonic and the plasmonic waveguides. (d) Quasi-TM mode profiles ($|E_y|$) supported by the different waveguide cross-sections, along the direction of propagation as they are denoted in (a).

offset was to minimize coupling losses by maximizing the mode overlap between the photonic and the plasmonic mode. In addition, the longitudinal offset was introduced as the means to evaluate possible metal deposition inaccuracies during fabrication. As can be seen, water filled also the longitudinal gap between the photonic and plasmonic waveguide at their interface section. The cross-sectional dimensions of the different waveguide configurations employed along the direction of propagation are shown in Fig. 1(c), while Fig. 1(d) depicts the corresponding quasi-TM mode profiles (dominant $|E_y|$). Our designs relied on a 360 nm thick Si_3N_4 waveguide on top of a 2.2 μm thick buried oxide, cladded with 600 nm of LTO, while the gold-based plasmonic stripes were selected to have a thickness of 100 nm with a 3 nm thick Ti layer underneath in order to facilitate gold adhesion and to avoid coupling of top surface plasmons into radiation modes in the buried oxide layer, absorbing any unwanted surface-plasmon modes at the bottom surface of gold [25]. We opted for a 360 nm × 800 nm Si_3N_4 strip based waveguide in order to ensure low-loss, single-mode quasi-TM polarised photonic mode propagation, allowing in this way for the deployment of more complex Si_3N_4 circuitry where still the proposed co-integration approach can be employed towards introducing plasmonic stripes at certain building blocks of the whole Si_3N_4 circuitry. The 360 nm × 800 nm Si_3N_4 strip waveguide was linearly tapered to a 7.5 μm wide photonic waveguide prior reaching the plasmonic segment in order to provide a photonic mode that is spatially matched with the plasmonic mode supported by the gold stripe. The width of the gold stripe was chosen to be 7 μm trading-off between low plasmonic propagation loss and compact footprint of the plasmonic waveguide while maintaining single mode-condition, hence allowing for compact layouts in view of their possible future employment in multichannel sensor configurations.

We conducted 3D FDTD simulations calculating the insertion loss of the proposed interface at 1.55 μm as a function of the VO and the LO between the photonic and the plasmonic waveguides. The insertion loss was determined after launching the quasi-TM mode of the tapered 7.5 μm-wide photonic waveguide and calculating the power that is coupled to the plasmonic mode. That was realized by utilizing the built-in mode expansion monitors of *Lumerical Solutions* software to ensure that the forward propagating power is isolated and to calculate only the power that is coupled into the surface-plasmon mode of interest. This data was then normalized with respect to the power of the photonic mode. During our parametric analysis and for each structural parameter variation, the mode expansion monitor was settled 2 μm away from the front-end of the gold stripe, as denoted by
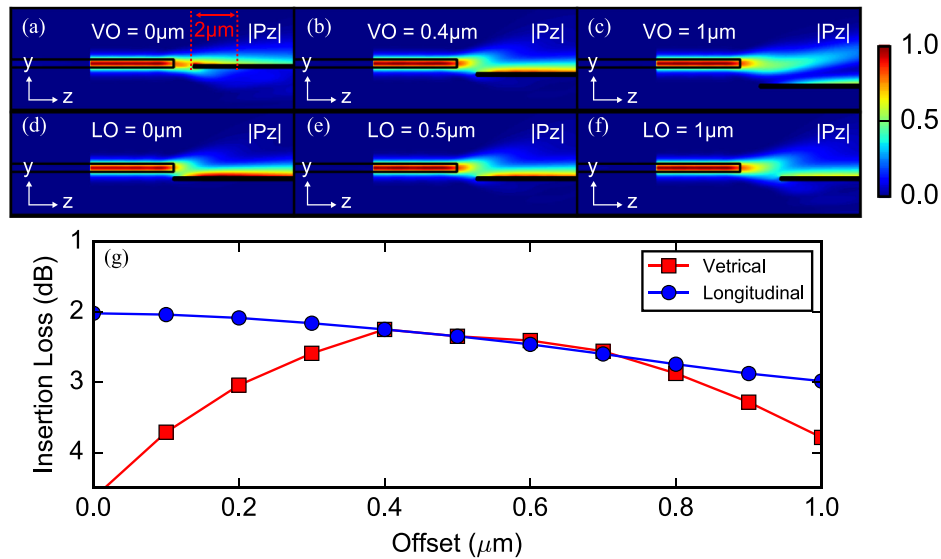
Fig. 2. (a), (b) and (c) norm of the Poynting vector $|P_z|$ along the direction of propagation for a longitudinal offset (LO) of 500 nm and vertical offset (VO) of 0, 0.4 and 1 μm, respectively. (d), (e) and (f) norm of the Poynting vector $|P_z|$ for a VO of 400 nm and LO of 0, 0.5 and 1 μm, respectively. (g) Simulated insertion loss per single transition of the butt-coupled interface as function of the VO (red-squares) for a fixed LO of 500 nm and the LO (blue-circles) for a fixed VO of 400 nm, between the photonic and the plasmonic waveguides.

the red dashed lines in Fig. 2(a). Given the negligible propagation losses induced by the damping of the SPP mode after such a short distance, the calculated insertion loss was not compensated for the propagation losses.

Simulations dictated a plasmonic propagation loss of 0.05 dB/μm corresponding to a characteristic surface-plasmon propagation length (L_{spp}) of 86 μm at 1.55 μm. Fig. 2(a)–(f) depict the norm of the Poynting vector ($|Pz|$) along the direction of propagation in a side-view for different combinations of VO and LO values. More specifically, Fig. 2(a), (b) and (c) show the norm of the Poynting vector with a fixed LO of 500 nm for VO values of 0, 0.4 and 1 μm, respectively. The Poynting vector plots that correspond to a fixed VO of 400 nm and LO values of 0, 0.5 and 1 μm are shown in Fig. 2(d), (e) and (f), respectively. We note that even in the extreme cases where either the VO or the LO reach 1 μm, the surface plasmon-mode on top of the gold stripe is still excited. We can also observe that surface-plasmon modes beneath the gold stripe are not excited even in the case of a VO of 0 nm (see Fig. 2(a)). The results obtained by a complete parametric analysis varying the VO between 0–1 μm for a fixed LO value and then varying the LO between 0–1 μm for a fixed VO value are shown in Fig. 2(g). 500 nm was used as the fixed LO value during VO parametric sweep in order to account for available lithography alignment resolution and the VO was varied from 0 to 1 μm with a step size of 100 nm. Based on the simulations results shown in Fig. 2(g), a minimum insertion loss of 2.2 dB at 1.55 μm was achieved for a VO of 400 nm. For VO values between 300 to 700 nm the insertion loss increases only by 0.3 dB. Keeping the VO fixed at lowest-loss value of 400 nm, the LO was varied between 0 to 1 μm with a step size of 100 nm in order to investigate its impact on the insertion loss value. For LO values of 0 and 1 μm the insertion loss reached 2 dB and 2.9 dB at 1.55 μm, respectively, indicating that the proposed interface exhibits a quite tolerant behavior to structural deviations in the range of a few hundred of nanometers around the optimal values of both the VO and LO. The refractive indices used in the simulations for the Si_3N_4, LTO, SiO_2 and water at 1.55 μm were 1.996, 1.444, 1.444 and 1.311-0.0001348i, respectively [34], [35]. During simulations we used the same refractive index value for both the LTO and the SiO_2 layers. The complex refractive indices used for gold and Ti at 1.55 μm were 0.26-11i and 4.04-3.82i, respectively [7], [35].
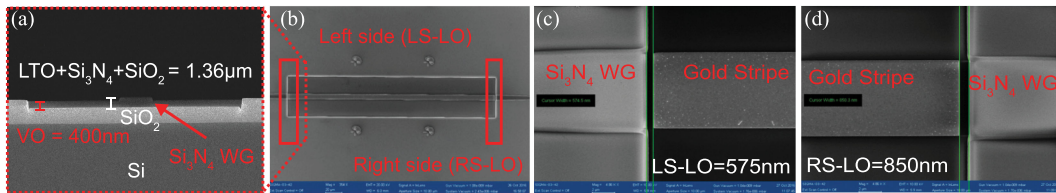
Fig. 3. SEM images of the plasmo-photonic interface. (a) Cross-sectional view through the cavity (along the red dashed curve) before the gold stripe deposition. The Si_3N_4 waveguide can be seen in the center. The depth of the cavity is 1.36 μm. LTO, Si_3N_4 and SiO_2 are etched in one process step. (b) Top-view of the cavity wherein the 7 μm wide by 250 μm long gold stripe is recessed (c) and (d) close-up top-view for the left and right hand side of the fabricated interface showing the actual longitudinal offset, respectively.

3. Fabrication and Characterization

The waveguide technology is based on standard 6" silicon wafer substrates with 2.2 μm of thermally grown SiO_2 and 360 nm Si_3N_4 as waveguide layer. The Si_3N_4 layer was deposited in an LPCVD-based process. Markers, waveguide structures and GCs were defined by optical projection lithography with a CANON i-line stepper tool. Reactive-ion-etching (RIE) based on CHF_3 and He chemistry has been used for the structure transfer of the waveguides. Afterwards, 600 nm of SiO_2 were deposited in a low temperature LPCVD furnace (LTO). A subsequent annealing process for several hours at 1000 °C minimized hydrogen content and absorption of the LTO cladding to reduce the waveguide propagation losses. In this way, the cladding becomes more condensed through the annealing and does not store humidity later on. Following Si_3N_4 waveguide processing, the cavities for the plasmonic material were defined by the i-line stepper tool and etched 1.36 μm deep through LTO, Si_3N_4 and SiO_2 as well by RIE with CHF_3 and He chemistry. The minimum critical dimensions achievable by the i-line stepper litho processes are 500 nm. Fig. 3(a) shows a cross-sectional scanning-electron-microscope (SEM) image of the cavity before the gold stripe deposition.

This lithography approach enables high throughput fabrication for photonic integrated circuits by using a step-and-repeat lithography system. Critical dimensions are matched to the resolution of i-line stepper lithography, hence the mask costs are comparably low to Deep-Ultra-Violet (DUV) stepper and phase shifter masks. The reproducibility and alignment of the projection lithography is excellent and no charging of the dielectric layers as in electron beam lithography has to be taken into account. The alignment from waveguide layer to cavities layer and also later to metal layer is more crucial than the critical dimensions which are rather big. In the final fabrication stage, the metallic plasmonic structures are deposited into the cavities by a lift-off process using e-beam lithography, thermal evaporation of gold and lift-off dissolution in a standard remover bath. The target thickness for gold was 100 nm. A 3 nm thick titanium layer was deposited by e-gun evaporation prior to gold for an improved adhesion of gold on the sample. To achieve a good lift-off in the unusual condition defined by the presence of the ~1 μm deep recess, the thickness of the Polymethylmethacrylate (PMMA) resist used for lithography was increased to 590 nm and the lithography exposure dose increased accordingly to 300 μC/cm^2 at 20 keV. In the lithography step, alignment was based on the recognition of the markers that were previously created in the silicon nitride layer covered with LTO. Fig. 3(b) illustrates a top-view of a test structure of a plasmonic waveguide interfaced at its both facets with respective Si_3N_4 waveguides. SEM inspection revealed that the actual values for the LO were larger than the originally targeted 500 nm, as shown in the close-up view of the left and right-side interfaces in Fig. 3(c) and (d), respectively.

Fig. 4(a) depicts the developed test structures for the characterization of the proposed interface. These test structures included: a reference structure comprising a 1 cm long straight Si_3N_4 waveguide with two 100 μm long linear tapers in the middle, interconnected to each other via 1 μm long and 7.5 μm wide waveguide. The interface test structures accommodate 7 μm wide gold stripes with variable gold length (20, 100, 150 and 250 μm) for cut-back measurements, with the metallic
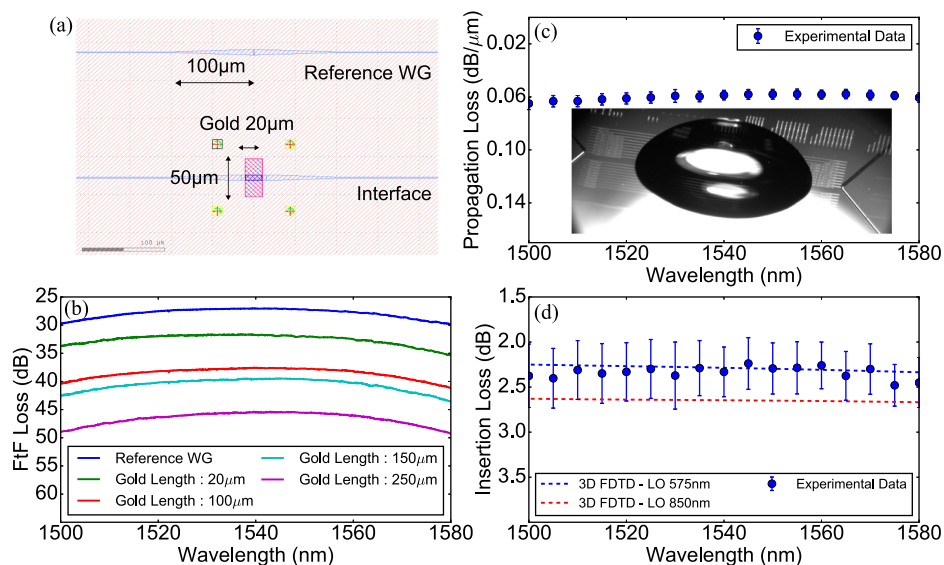
Fig. 4. (a) Mask layout depicting the developed test structures for the characterization of the proposed interface. The targeted LO for all the interface test structures is 500 nm. (b) Fiber-to-Fiber loss budget for the measured test structures (c) Propagation loss of the plasmonic mode as function of wavelength in water. Inset shows a drop of water on top of the sample. (d) Experimental and theoretical results for the insertion loss of the proposed interface, per single transition, as a function of wavelength.

stripe being deposited in a 50 μm wide cavity, as shown in Fig. 4(a). Measurements were carried out by sweeping the wavelength of a tunable laser source from 1.5 μm to 1.58 μm and by using a polarization controller for ensuring the coupling of TM-polarized light into the Si_3N_4 waveguides. Fig. 4(b) shows the fiber-to-fiber (FtF) loss budget for the characterized test structures as a function of wavelength. The propagation losses of the plasmonic mode in water were measured for wavelengths ranging from 1.5 μm to 1.58 μm with a step of 5 nm, performing least-squares linear fitting on the FtF loss budget data of the interface test structures with increasing gold length. Fig. 4(c) shows the plasmonic propagation loss in water as a function of wavelength, revealing 0.058 dB/μm losses at 1.55 μm that correspond to an L_{spp} of 75 μm, close to the theoretically predicted value of 86 μm. The error bars correspond to the standard deviation deduced from the linear fitting process. The inset of Fig. 4(c) depicts a drop of water on top of the sample. To calculate the insertion loss of the proposed photonic-to-plasmonic interface per single transition, the FtF losses of the reference Si_3N_4 waveguide structure were subtracted from the intercept values obtained by this linear fitting process and the resulting loss value was divided by a factor of two. The experimental insertion loss, per single transition, derived from this calibration process is depicted by the blue scatter points with the error bars in Fig. 4(d), showing a value of 2.3 ± 0.3 dB at 1.55 μm. Fig. 4(d) shows also the numerical results obtained from broadband simulations for a single transition, when using LO values between the photonic and plasmonic waveguides identical to the values that were finally employed in the fabricated samples via SEM inspection. Broadband simulations were performed taking into account the dispersive properties of the considered metals, revealing interface losses of 2.3 dB for LO = 575 nm and 2.8 dB for LO = 850 nm that yield an average loss value of 2.55 dB at 1550 nm, being close to the experimentally measured data.

Following the good agreement between theory and experiment for the butt-coupled interface and the plasmonic propagation losses in aqueous environment, the accumulated phase change per refractive index unit has been calculated theoretically over a propagation distance equal to an L_{spp} length of 86 μm. This investigation provides an insight into the potential of this plasmo-photonic waveguide platform in biochemical sensing applications when deployed in interferometric arrangements. By using the commercial-grade simulator eigenmode solver of *Lumerical Solutions* software [36], a refractive index change of $\Delta n = 0.01$ was introduced to the overlying water and

the numerical results revealed a plasmonic mode at 1.55 μm with an effective index n_{eff} of 1.327, increased by $\triangle n_{eff} = 0.01$ compared to its initial value with unperturbed aqueous solution. Using this $\triangle_{neff}$ value, the accumulated phase change over a length of L_{spp} is calculated to be 1.13π for a $\Delta n = 10^{-2}$, which translates into $113\pi/RIU/L_{spp}$ or, alternatively, into $1.25\pi/RIU/\mu$m, with typical experimental phase change sensitivity values of photonic sensing waveguides hardly exceeding $0.27\pi/RIU/\mu$m [19] even when more sensitive photonic slot configurations, instead of evanescent wave photonic sensing waveguides, are used.

4. Conclusion

We have demonstrated, for the first time to the best of our knowledge, a butt-coupled interface between Si_3N_4 silicon nitride waveguides and gold-based plasmonic stripes in aqueous environment reporting an experimentally measured insertion loss of 2.3 ± 0.3 dB at 1.55 μm per singe transition, with an L_{spp} of 75 μm. Good agreement between theoretically predicted and experimentally measured values is obtained, with numerical analysis revealing also a ± 200 nm VO tolerance for an excessive loss of only 0.7 dB and an insertion loss difference of 0.9 dB within a LO range of 0–1 μm. This suggests a high potential towards a fabrication-tolerant co-integrated plasmo-photonic waveguide platform that can be eventually employed in biochemical sensing applications.

References

[1] D. K. Gramotnev and S. I. Bozhevolnyi, "Plasmonics beyond the diffraction limit," *Nature Photon.*, vol. 4, no. 2, pp. 83–91, 2010.
[2] R. Buckley and P. Berini, "Figures of merit for 2D surface plasmon waveguides and application to metal stripes," *Opt. Exp.*, vol. 15, no. 19, pp. 12174–12182, 2007.
[3] L. Liu, Z. Han, and S. He, "Novel surface plasmon waveguide for high integration," *Opt. Exp.*, vol. 13, no. 7, pp. 6645–6650, 2005.
[4] S. I. Bozhevolnyi, V. S. Volkov, E. Devaux, J. Y. Laluet, and T. W. Ebbesen, "Channel plasmon subwavelength waveguide components including interferometers and ring resonators," *Nature*, vol. 440, no. 7083, pp. 508–511, 2006.
[5] P. Berini, R. Charbonneau, N. Lahoud, and G. Mattiussi, "Characterization of long-range surface-plasmon polariton waveguides," *J. Appl. Phys.*, vol. 98, no. 4, 2005, Art. no. 043109.
[6] M. Ono *et al.*, "Deep-subwavelength plasmonic mode converter with large size reduction for Si-wire waveguide," *Optica*, vol. 3, no. 9, pp. 999–1005, 2016.
[7] J. Weeber *et al.*, "Characterization of CMOS metal based dielectric loaded surface plasmon waveguides at telecom wavelengths," *Opt. Exp.*, vol. 25, pp. 394–408, 2017.
[8] S. Papaioannou *et al.*, "A 320 Gb/s-throughput capable 2x2 silicon-plasmonic router architecture for optical interconnects," *J. Lightw. Technol.*, vol. 29, no. 21, pp. 3185–3195, 2011.
[9] D. Kalavrouziotis *et al.*, "0.48Tb/s (12x40Gb/s) WDM transmission and high-quality thermo-optic switching in dielectric loaded plasmonics," *Opt. Exp.*, vol. 20, pp. 7655–7662, 2012.
[10] S. Papaioannou *et al.*, "Active plasmonics in WDM traffic switching applications," *Sci. Rep.*, vol. 2, pp. 652–666, 2012.
[11] C. Hoessbacher *et al.*, "Plasmonic modulator with >170 GHz bandwidth demonstrated at 100 GBd NRZ," *Opt. Exp.*, vol. 25, no. 3, pp. 1762–1768, 2017.
[12] J. Gosciniak, V. S. Volkov, S. I. Bozhevolnyi, L. Markey, S. Massenot, and A. Dereux, "Fiber-coupled dielectric-loaded plasmonic waveguides," *Opt. Exp.*, vol. 18, no. 5, pp. 5314–5319, 2010.
[13] J. Gosciniak *et al.*, "Thermo-optic control of dielectric-loaded plasmonic waveguide components," *Opt. Exp.*, vol. 18, no. 2, pp. 1207–1216, 2010.
[14] N. Pleros *et al.*, "Tb/s switching fabrics for optical interconnects using heterointegration of plasmonics and silicon photonics: The FP7 PLATON approach," in *Proc. 2010 23rd Annu. Meet. IEEE Photon. Soc.*, Denver, CO, 2010, pp. 165–166.
[15] M. Ayata *et al.*, "High-speed plasmonic modulator in a single metal layer," *Science*, vol. 358, no. 6363, pp. 630–632, 2017.
[16] B. Liedberg, C. Nylander, and I. Lundstrom, "Surface plasmon resonance for gas detection and biosensing," *Sens. Actuators B*, vol. 4, pp. 299–304, 1983.
[17] J. Homola, "Surface plasmon resonance sensors for detection of chemical and biological species," *Chem. Rev.*, vol. 108, no. 2, pp. 462–493, 2008.
[18] G. A. Lopez., M. Estevez, M. Soler, and L. M. Lechuga, "Recent advances in nanoplasmonic biosensors: Applications and lab-on-a-chip integration," *Nanophotonics*, vol. 6, no. 1, pp. 123–136, 2017.
[19] A. Fernández Gavela, D. Grajales García, J. C. Ramirez, and L. M. Lechuga, "Last advances in silicon-based optical biosensors," *Sensors (Basel)*, vol. 16, no. 3, pp. 285–300, 2016.
[20] O. Tsilipakos *et al.*, "Interfacing dielectric-loaded plasmonic and siliconphotonic waveguides: theoretical analysis and experimental demonstration," *IEEE J. Quantum Electron.*, vol. 48, pp. 678–687, 2012.

[21] C. Delacour *et al.*, "Efficient directional coupling between silicon and copper plasmonic nanoslot waveguides: toward metal−oxide−silicon nanophotonics." *Nano Lett.*, vol. 10, no. 8, pp. 2922–2926, 2010.
[22] Q. Li and M. Qiu, "Structurally-tolerant vertical directional coupling between metal-insulator-metal plasmonic waveguide and silicon dielectric waveguide," *Opt. Exp.*, vol. 18, no. 15, pp. 15531–15543, 2010.
[23] A. Melikyan, M. Kohl, M. Sommer, C. Koos, W. Freude, and J. Leuthold, "Photonic-to-plasmonic mode converter," *Opt. Lett.*, vol. 39, no. 12, pp. 3488–3491, 2014.
[24] C. T. Chen, X. Xu, A. Hosseini, Z. Pan, and R. T. Chen, "High efficiency silicon strip waveguide to plasmonic slot waveguide mode converter," *Proc. SPIE*, vol. 9368, 2015, Art. no. 936809.
[25] R. M. Briggs, J. Grandidier, S. P. Burgos, E. Feigenbaum, and H. A. Atwater, "Efficient coupling between dielectric-loaded plasmonic and silicon photonic waveguides," *Nano Lett.*, vol. 10, no. 12, pp. 4851–4857, 2010.
[26] S. Zhu, G. Lo, and D. Kwong, "Silicon nitride based plasmonic components for CMOS back-end-of-line integration," *Opt. Exp.*, vol. 21, no. 20, pp. 23376–23390, 2013.
[27] R. Wan, F. Liu, X. Tang, Y. Huang, and J. Peng, "Vertical coupling between short range surface plasmon polariton mode and dielectric waveguide mode," *Appl. Phys. Lett.*, vol. 94, no. 14, 2009, Art. no. 41104.
[28] F. Liu *et al.*, "Extremely high efficient coupling between long range surface plasmon polariton and dielectric waveguide mode," *Appl. Phys. Lett.*, vol. 95, no. 9, 2009, Art. no. 091104.
[29] X. Sun, D. Dai, L. Thylén, and L. Wosinski, "High-sensitivity liquid refractive-index sensor based on a Mach-Zehnder interferometer with a double-slot hybrid plasmonic waveguide," *Opt. Exp.*, vol. 23, no. 20, pp. 25688–25699, 2015.
[30] B. Y. Fan, F. Liu, Y. X. Li, Y. D. Huang, Y. Miura, and D. Ohnishi, "Refractive index sensor based on hybrid coupler with short-range surface plasmon polariton and dielectric waveguide," *Appl. Phys. Lett.*, vol. 100, no. 11, 2012, Art. no. 111108.
[31] Lumerical Solutions, Inc. [Online]. Available: http://www.lumerical.com/tcad-products/fdtd/
[32] G. Dabos *et al.*, "TM grating couplers for low-loss LPCVD based Si$_3$N$_4$ waveguide platform," in *Proc. Conf. Lasers Electro-Opt., OSA Tech. Dig. (Online)*, 2017, Paper JTh2A.103.
[33] G. Dabos *et al.*, "TM grating coupler on low-loss LPCVD based Si$_3$N$_4$ waveguide platform," *Opt. Commun.*, vol. 405, pp. 35–38, 2017.
[34] K. Luke, Y. Okawachi, M. R. E. Lamont, A. L. Gaeta, and M. Lipson, "Broadband mid-infrared frequency comb generation in a Si$_3$N$_4$ microresonator," *Opt. Lett.*, vol. 40, pp. 4823–4826, 2015.
[35] D. W. Lynch and W. R. Hunter, *Handbook of Optical Constants of Solids*, E. D. Palik, Ed. San Francisco, CA, USA: Academic, 1985.
[36] Lumerical Solutions, Inc. [Online]. Available: http://www.lumerical.com/tcad-products/mode/